^{219}Fr, a transitional reflection asymmetric nucleus

C. F. Liang and P. Paris
Centre de Spectrométrie Nucléaire et de Spectrométrie de Masse, Bâtiment 104, 91405 Campus Orsay, France

J. Kvasil and R. K. Sheline
Departments of Chemistry and Physics, Florida State University, Tallahassee, Florida 32306
(Received 8 November 1990)

Mass-separated sources of ^{223}Ac (separated as AcF_2^+) were used to study the level structure of ^{219}Fr following alpha decay. The levels in ^{219}Fr are interpreted in terms of $K=\frac{1}{2}^{\pm}$, $\frac{3}{2}^{\pm}$, and $\frac{5}{2}^{\pm}$ parity doublet bands which have a natural theoretical explanation in terms of reflection asymmetric models. The $\frac{9}{2}^-$ ground-state member of the $K=\frac{1}{2}^-$ band in ^{219}Fr can be understood in terms of both reflection asymmetry and the collapse of the quadrupole-octupole Nilsson orbitals towards the $h_{9/2}$ orbitals of spherical symmetry. Comparison of the $K=\frac{1}{2}^-$ ground-state bands in ^{219}Fr and ^{221}Fr reveals the details of this transformation. Theoretical analysis of the microscopic structure of several of the positive-parity bands indicates the presence of important Nilsson configurations arising from the shell below.

INTRODUCTION

^{219}Fr is in a strategic position in the nuclear periodic table. It is on the edge of the region of reflection asymmetry. Other odd-A nuclei in this region often seem to exhibit a weak-coupling spectroscopy in which the odd proton or neutron couples with collective states of the even-even reflection asymmetric core. This is true, for example, of ^{219}Ra [1] and ^{219}Ac [2,3] with ^{218}Ra [4–6] acting as the core. It is also true of ^{217}Fr [7], although the spectroscopy is not so well developed. In all of these cases, one observes sets of states with increasing spins and alternating parities forming a band (e.g., $\frac{9}{2}^+, \frac{11}{2}^-, \frac{13}{2}^+, \frac{15}{2}^-, \ldots,$), where the states are connected by enhanced $E1$ transitions and energies, and transition probabilities bear a striking resemblance to the ground-state rotational band of ^{218}Ra. On the other hand, ^{221}Fr [8] and ^{221}Ra [9] have the typical strong-coupling spectra expected of quadrupole-octupole deformed systems. The spectroscopy of ^{217}Fr and ^{219}Ra is particularly anomalous. In addition to the heavy-ion spectroscopy leading to the weak-coupled band structure, there are states observed in these nuclei through alpha decay [10,11]. However, no energy differences in the levels of the alpha populated levels correspond to the weak-coupled band structures in the same nucleus. It is almost as if there were two separate spectroscopies. It is to be hoped that the study of ^{219}Fr can provide additional data with which to understand this anomaly.

Furthermore, with only five protons and six neutrons beyond the double closed shell of ^{208}Pb, ^{219}Fr lies in the region where quadrupole-octupole deformation is shrinking toward spherical symmetry. The octupole and quadrupole deformations are expected to be similar with $\epsilon_2 \simeq \epsilon_3 \simeq 0.08$. The symmetry breaking, in going from a spherical system to a quadrupole-octupole deformed system in this transitional nucleus, is therefore an important test of nuclear models.

A shorter preliminary version of this paper was given at the Oak Ridge International Conference on Nuclear Structure in the Nineties [12].

EXPERIMENTAL METHODS AND RESULTS

We have studied the level structure of ^{219}Fr by observing the alpha decay of mass-separated $^{223}AcF_2^+$ and the accompanying gamma and electron transitions. A target of approximately 10 g of thorium-cerium alloy was heated to 1100 °C and bombarded with ~ 1 μA of 200-MeV protons on three separate occasions, varying from 30 to 48 h. A flow of CF_4 vapor was passed over the target continuously during the bombardment. $^{223}AcF_2$ ions (mass 261) were mass separated using the Orsay ISOCELE separator. The activity collected varied from 1×10^4 to 5×10^5 ions/s. This method [13] produces ^{223}Ac ions without the contamination of other volatile Ra, Fr, and Rn isotopes. A tape transport system moved the collected 2.2-min ^{223}Ac activity into two different experimental setups. In the first experiment, the activity was moved between an alpha and a gamma detector in a 180° close geometry. The alpha detector had a resolution better than 15 keV for ^{223}Ac alpha particles, while the gamma detector had a resolution of approximately 600 eV at 100 keV. Singles alpha and gamma spectra and 4K-4K (4096×4096 channels) alpha-gamma coincidence measurements were recorded simultaneously.

In the second experiment, the tape transport system moved the collected ^{223}Ac activities into a magnetic selector where electrons were deflected by a uniform magnetic field and caused to impinge onto a cooled 6-mm-thick Si(Li) detector. Two additional detectors for gamma rays and alpha particles were also available for coincidence measurements. Singles alpha and electron spectra and 4K-4K alpha-electron and electron-gamma coincidence measurements were recorded simultaneously. In all of the above experiments, measurement cycles were 2 min,

in accord with the 2.2-min half-life of ^{223}Ac.

The coincidence alpha spectrum of ^{223}Ac and some of its daughter products are shown in Fig. 1. The alpha energies in keV, used to label the alpha peaks in Fig. 1, are the more accurate values of Leang [14] who used a magnetic spectrograph for his measurement. The ^{211}Bi and ^{219}Fr impurity peaks are also labeled. It is clear, from these spectra, that ^{223}Ac is relatively pure. This facilitates fairly simple alpha-gamma and alpha-electron coincidence measurements. Portions of the gamma-ray spectrum coincident with all alpha particles of ^{223}Ac are shown in Fig. 2. Gamma rays in ^{219}Fr are labeled with their energies in keV, while x rays of Fr and Tl from ^{211}Bi are specifically labeled in Fig. 2. The internal conversion electron spectrum coincident with the alpha-particle group of 6563 keV is shown in Fig. 3. Individual electron lines are labeled in keV, and the L, M, and N lines are indicated. In all, 52 gamma rays have been observed for ^{219}Fr. Multipolarities for 17 of the gamma rays have been determined. Table I lists all gamma rays observed, together with their energies, intensities, and multipolarities. The assignments in the ^{219}Fr level scheme together with the rationale for these assignments are also given.

A very powerful aid in the construction of the level scheme was the systematic comparison of gamma-ray and electron spectra, coincident with alpha particles as the alpha-particle energies are decreased, corresponding to moving up in excitation energy in the ^{219}Fr level structure. Figure 4 shows a sequence of gamma-ray spectra coincident with alpha spectra of increasing energy. These spectra clearly show gamma rays growing in and out as certain levels in ^{219}Fr are populated by alpha particles. To the extent that levels in ^{219}Fr are not too close together, it allows population of individual levels and the observation of their depopulation separate from the rest of the level scheme. In those cases where levels are too close together, the gamma-ray energies themselves are necessary to distinguish between the levels.

While most of the details of the assignments of spins and parities are given in Table I, it is important to note several additional factors. The ground state and 490.3-keV state have previously been assigned [10] spin parity $\frac{9}{2}^-$ and $\frac{5}{2}^-$, respectively. The $\frac{5}{2}^-$ assignment to the 490.3-keV state is based on the low alpha-decay hindrance factor (2.9) from the known $\frac{5}{2}^-$ ground state of ^{223}Ac [15]. In addition, a rotational band built on the 490.3-keV state, based on $J(J+1)$ model considerations and the expected sequence of hindrance factors, has been proposed [10]. Assignments into bands are based on model considerations and plausibility arguments from the tendencies of gamma-ray depopulation within bands. It should, however, be noted that there is considerable Coriolis coupling between the $K=\frac{1}{2}^-$ and $\frac{3}{2}^-$ and between the $K=\frac{1}{2}^+$ and $\frac{3}{2}^+$ bands (see Discussion). In some cases this makes the assignments of levels to bands somewhat arbitrary. Finally, it should be noted that the assignment of spin parities to the higher-lying levels (particularly those with the smallest alpha populations) is more tentative. This uncertainty results because, with

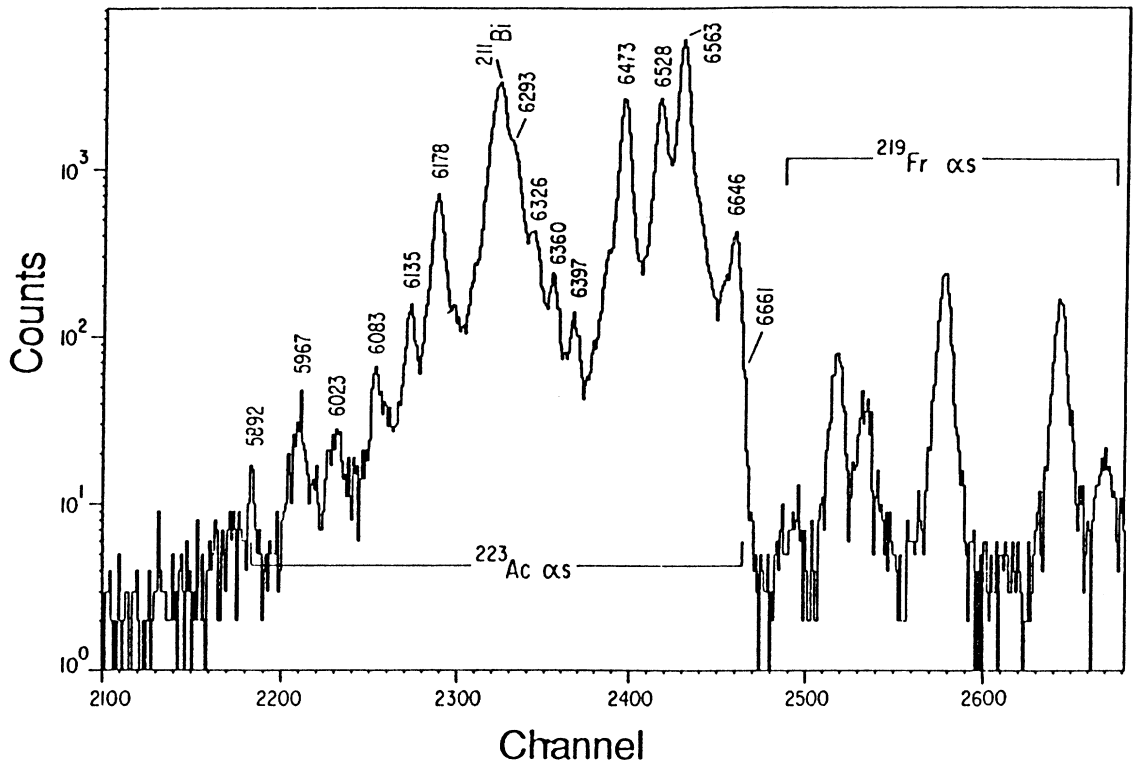

FIG. 1. Alpha spectrum of ^{223}Ac in coincidence with all gamma rays into levels in ^{219}Fr. Energies of the major alpha groups taken from Leang [14] are given in keV. Alpha groups from ^{219}Fr, which is in secular equilibrium with ^{223}Ac, are also shown.

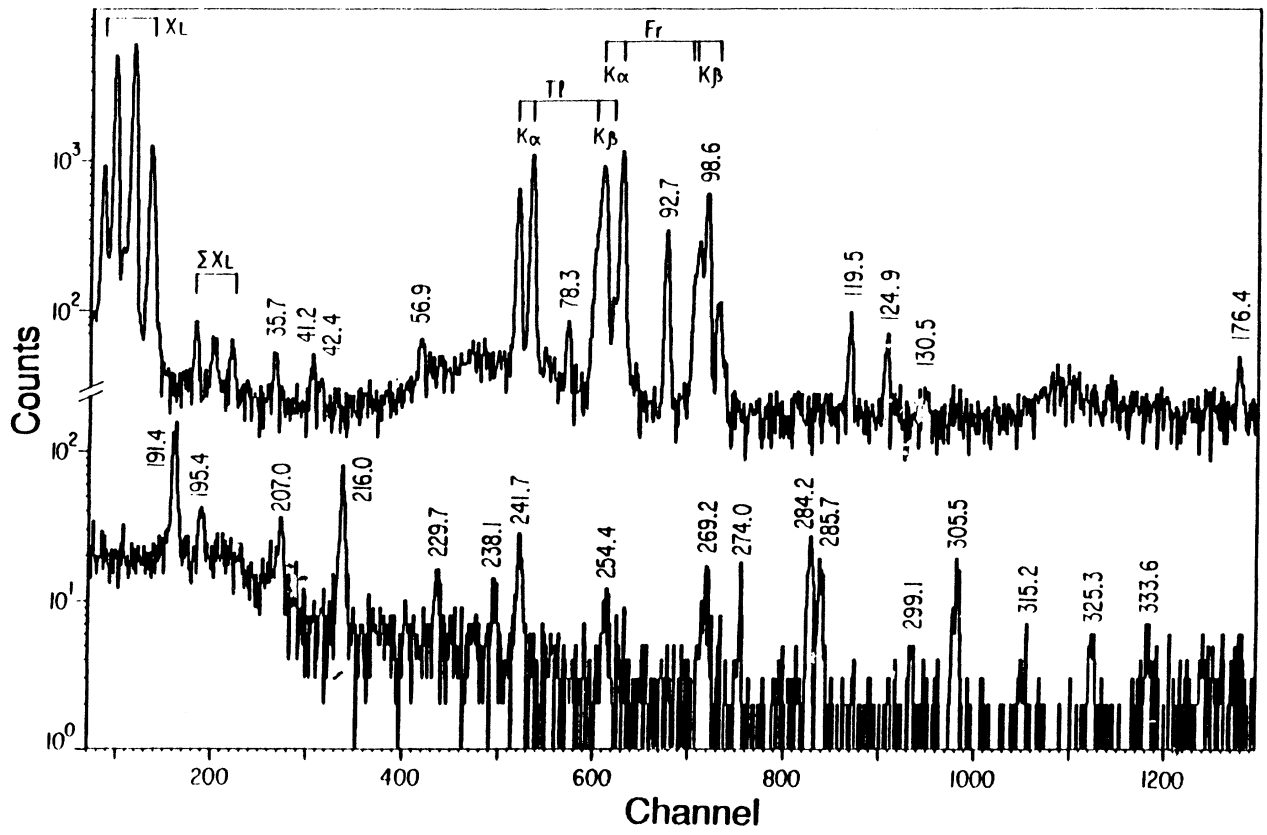

FIG. 2. Portion of the gamma spectrum in coincidence with alpha particles of 5892–6646 keV from ^{223}Ac and 6279 keV of ^{211}Bi. Gamma transitions in ^{219}Fr are given in keV, and K x rays of Fr and Tl are indicated.

decreasing population of the levels, the resulting decreased depopulation of the levels makes the conclusions which can be drawn less certain. In particular, spin parities of the levels of 706 and 779 keV are especially speculative. The suggested spin parities are mostly based on the low alpha-decay hindrance factors and the energies of these states relative to the 490.3-keV $\frac{5}{2}^-$ band. It should also be noted that the 72.8-keV gamma ray between the 779- and 706-keV levels is in coincidence with the 5892-keV alpha particle populating the 779-keV level. However, the placements of the 171.7-keV gamma ray depopulating the 706-keV level and the 82.4-keV gamma ray

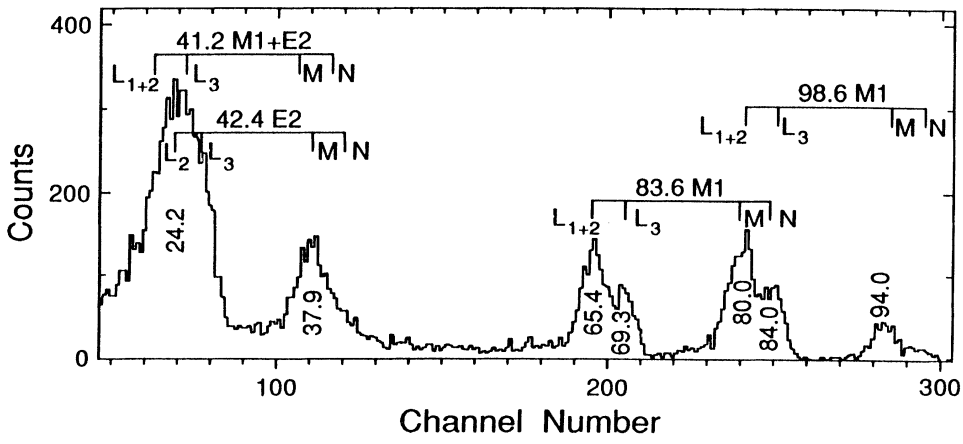

FIG. 3. Portion of the internal conversion spectrum coincident with the alpha particle group of 6563 keV in ^{223}Ac. Electron energies of the lines are given in keV, and L, M, and N assignments are indicated.

TABLE I. Gamma-ray transitions in ^{219}Fr. Energies of the gamma rays in keV; intensities, multipolarities (when known), and the assignment in the level scheme are given. The gamma rays observed are those in coincidence with the alpha particles following the decay of ^{223}Ac.

E_γ (keV)	(ΔE_γ)	Thesis Leang (1969)	$I_\gamma(\Delta I_\gamma)/100\alpha$	Multipol.	Levels Initial → Final (keV) (keV)	Remarks
35.7	(0.1)		0.028(4)	$M1$	134.4→98.55	$M1$ from I balance
41.15	(0.1)		0.024(4)	$M1+E2$	56.15→15.0	mixed $M1+E2$ for I balance
42.4	(0.1)		0.013(3)	$E2$	98.55→56.2	$E2$ for I balance
56.95	(0.2)		0.038(6)	($E1$)	191.4→134.4	($E1$) from decay scheme
64.4	(0.3)		~0.02		333.6→269.2	E_γ; gate on α to 340
66.0	(0.5)		0.011(7)		(81→15.0)	No expt. argument; E_γ only
(72.8)		73(1)	<0.01		779→706	α to 779 gate on 172γ
78.25	(0.1)		0.055(7)	($M1$)	134.4→56.15	($M1$) from decay scheme
(82.4)			<0.01		(589.1→506.7)	mixed with X_k $T1$
83.55	(0.1)	84(1)	0.58(4)	($M1$)	98.55→15.0	$M1$ from e^-L_{1+2}/L_3
89.6	(0.2)		0.05(1)		305.5→216.0	E_γ only
92.71	(0.05)	93 (1)	0.39(2)	$E1$	191.3→98.55	$E1$ from I balance
98.58	(0.05)	99 (1)	0.90(2)	$M1$	98.55→0	$M1$ from e^-L_{1+2}/L_3
101.1	(0.2)		0.04(1)			not assigned
119.4	(0.1)	120 (2)	0.11(1)	$M1$	134.4→15.0	$M1$ from I balance
124.8	(0.1)	126 (2)	0.09(1)	$M1$	139.8→15.0	$M1$ from I balance
126.4	(0.2)		~0.01		432.1→305.6	gate on α to 430
(130.5)			0.02(1)			not assigned
134.6	(0.3)		~0.01		269.2→134.4	E_γ; gate on α to 270
171.7	(0.3)		0.02(1)		706→534	E_γ only
176.3	(0.2)	176 (2)	0.11(2)	$E1+(M2)$	191.3→15.0	<5% $M2$ necessary for I balance
191.3	(0.1)	192 (1)	0.59(4)	$E1+(M2)$	191.3→0	<5% $M2$ necessary for I balance
195.4	(0.2)		0.12(2)	$E1$	210.4→15.0	$E1$ from I balance
199.3	(0.4)		0.03(2)			not assigned
205.7	(0.3)		0.04(2)		340.3→134.4	energy fit only
207.0	(0.2)	207 (2)	0.19(4)	($M1$)	305.6→98.55	decay scheme +I balance
216.0	(0.1)	216 (1)	0.37(4)	$E1$	216.0→0	two places for this transition gate on α to 432
216.1	(0.2)		0.04(2)		432.1→216.0	
229.7	(0.2)		0.07(1)		369.6→139.8	E_γ and gate on α to 370
238.1	(0.2)		0.07(1)		372.4→134.4	E_γ and gate on α to 370
241.7	(0.2)		0.18(2)	($E1$)	340.3→98.55	E_γ and gate on α to 340
254.4	(0.3)		0.07(2)		269.2→15.0	E_γ and gate on α to 270
269.2	(0.1)	268(2)	0.10(2)		269.2→0	E_γ and gate on α to 270
274.0	(0.2)		0.05(1)		372.4→98.55	E_γ and gate on α to 372
279.8	(0.3)		0.03(1)		490.3→210.4	seen only with gate on α to 490
284.2	(0.1)		0.20(2)	($E1$)	340.3→56.15	($E1$) from decay scheme
285.7	(0.1)		0.13(2)		384.3→98.55	E_γ and gate on α to 400
299.1	(0.3)		0.03(1)		490.3→191.3	E_γ and gate on α to 500
305.5	(0.1)	306 (2)	0.18(2)		305.6→0	E_γ and gate on α to 305
315.2	(0.3)		0.01		506.6→191.3	seen only with gate on $\propto$ to 500
325.3	(0.1)		0.05(2)		340.3→15.0	energy fit only
333.5	(0.1)		0.11(4)		333.6→0	E_γ and gate on α to 350
(341.0)			0.05(3)			not assigned
357.4	(0.1)	359(2)	0.18(3)		372.4→15.0	E_γ and gate on α to 380
372.4	(0.1)	373(2)	0.16(3)		372.4→0	E_γ and gate on α to 380
374.8	(0.2)		0.06(1)		374.8→0	E_γ and gate on α to 380 (new level)
434.2	(0.1)	433(2)	0.53(5)		490.3→56.15	E_γ and gate on α to 500
462.2	(0.5)		0.04(2)		462.2→0	gate on $\propto$ to 450 (new level)
475.2	(0.1)	477(2)	0.27(4)		490.3→15.0	E_γ and gate on α to 500
506.6	(0.5)		0.03(2)		506.6→0	gate on α to 500
518.8	(0.4)		0.09(3)		533.8→15.0	E_γ and gate on α to 550
530.0	(0.5)		0.03(2)		530.0→0	gate on α to 550 (new level)
X_k	(Fr)		2.90(5)			

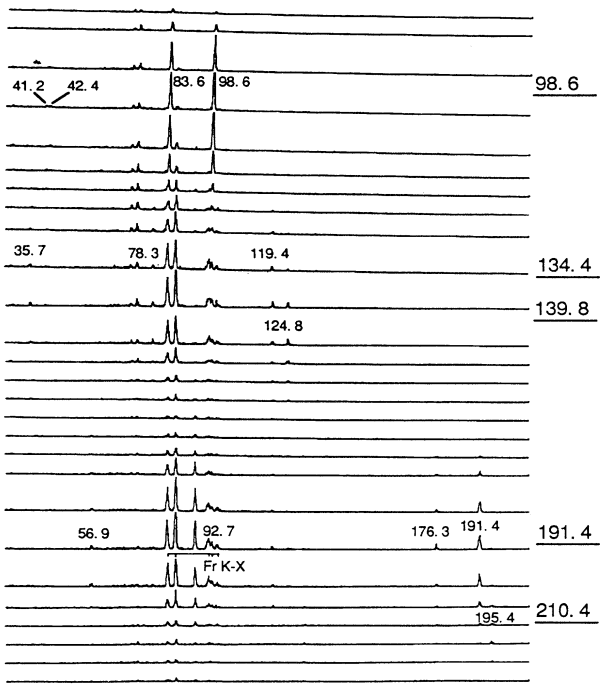

FIG. 4. Series of ^{219}Fr gamma spectra coincident with decreasing ^{223}Ac alpha energies from top to bottom with gamma energies in keV as indicated. The corresponding increasing energies (keV) of excitation in ^{219}Fr resulting from the alpha population are given to the extreme right of the figure.

depopulating the 589-keV level are based on energy fits only and therefore are tentative. In summary, we emphasize again the fact that the higher in energy we go in the level scheme and the smaller the alpha population, the more tentative the level scheme.

The resulting level scheme for ^{219}Fr, representing more than 99.5% of the alpha decay, is shown in Fig. 5. The energies of the levels in Fig. 5 are given to the left of each level and the spins and parities to the right. Also, to the right of each level, the energy in keV (and in parentheses the intensity in percent) of the alpha populating the level is given. In the case of the three levels near ~372 keV, only a single alpha population is observed. Gamma-ray transitions are shown as vertical arrows with their energies and, when known, their multipolarities. Bands are given as vertical arrays with the appropriate K quantum numbers. Those levels not assigned to bands are listed to the far right. The levels at 325 and 445 keV are shown as dashed lines. They are weakly populated directly in the alpha decay of ^{223}Ac, but no depopulation of the levels is observed.

DISCUSSION

The nucleus ^{219}Fr, with five protons and six neutrons more than the doubly closed-shell nucleus ^{208}Pb, would be expected to be difficult to understand using the shell model. Furthermore, it has 11 fewer nucleons than $A=230$ nuclei, which are normally considered to be the lightest nuclei which can be directly interpreted with the Nilsson model. Clearly, ^{219}Fr is in the transition region. It lies closest to the $A=220-230$ region, where reflection

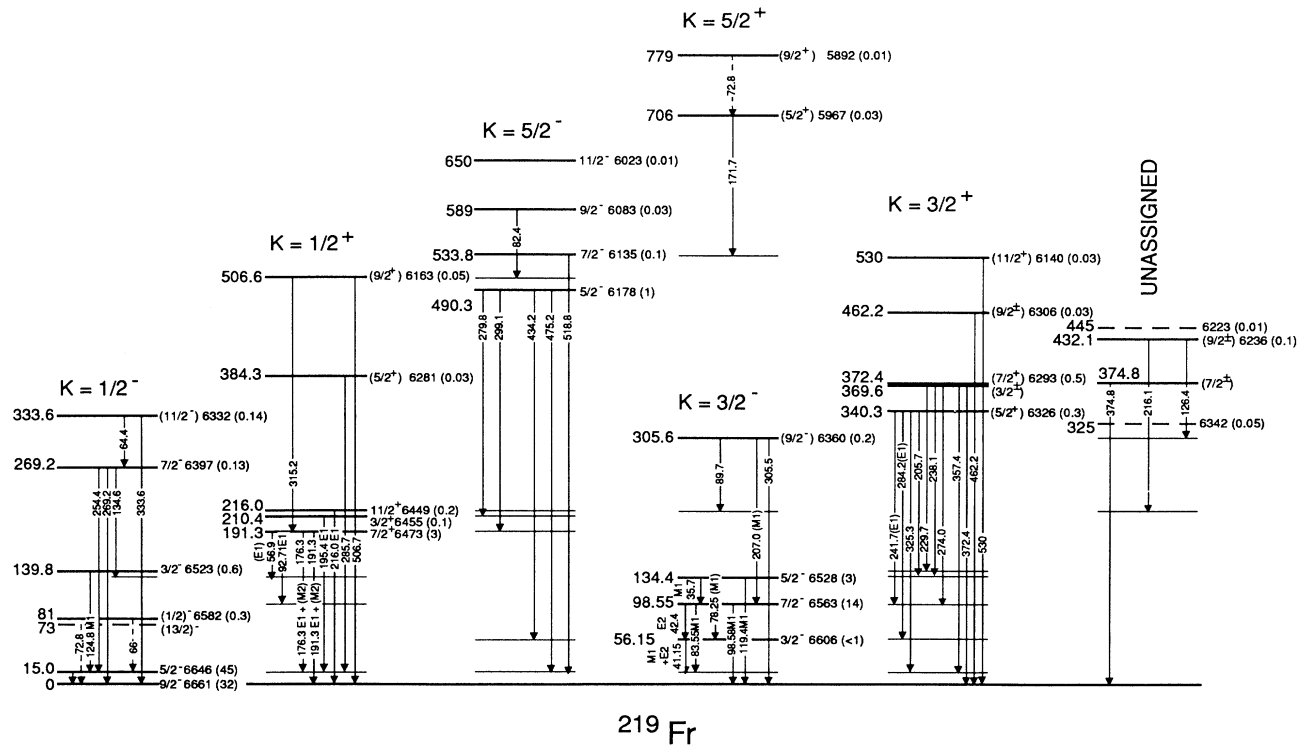

FIG. 5. Experimental level structure of ^{219}Fr, with energies of the levels, spins, and parities and the energy and intensity of the alphas populating each level. Gamma-ray transitions and multipolarities when known are also given. See text for more details.

asymmetry has been observed. In fact, ^{221}Fr, with two neutrons more than ^{219}Fr, has been interpreted [8,16] in terms of a reflection asymmetric model. In an odd-A reflection asymmetric system, we expect to observe parity doublet (PD) bands. These are rotational bands with the same spins, but opposite parities, which are reasonably close together in energy. In Fig. 5 the energies, spins, and parities of the levels in ^{219}Fr fit naturally into three sets of PD bands with $K=\frac{1}{2}^{\pm}$, $\frac{3}{2}^{\pm}$, and $\frac{5}{2}^{\pm}$. This is shown in Fig. 6, where the sets of PD bands are shown with double arrows. However, the PD splitting between the positive- and negative-parity bandheads is 191.4 keV for the $K=\frac{1}{2}^{\pm}$ PD bands, 267 keV for the $K=\frac{3}{2}^{\pm}$ PD bands, and 215.7 keV for the $K=\frac{5}{2}^{\pm}$ PD bands. This is larger than the usual PD splittings in the actinide region, although considerably smaller than the splittings expected for octupole vibrations. Since it involves all three sets of PD bands, it seems to be characteristic of this transitional region.

A second sign of reflection asymmetry would be the presence of decoupling parameters in the $K=\frac{1}{2}^{\pm}$ PD bands with the same absolute values, but with opposite signs. Each of the $K=\frac{1}{2}$ bands in ^{219}Fr has very anomalous spin sequences. If we take the $\frac{9}{2}^{-}$, $\frac{3}{2}^{-}$, and $\frac{7}{2}^{-}$ energies from the ground-state $K=\frac{1}{2}^{-}$ band, we calculate the inverse moment of inertia ($\hbar^2/2\mathcal{J}$) and the decoupling parameter (a) as 4.6 keV and 7.0, respectively. Using these parameters, we calculate -9.6 and 49.2 keV for the $\frac{5}{2}^{-}$ and $\frac{13}{2}^{-}$ states, in reasonable agreement for a transitional nucleus with the observed energies of 15.0 and 73 keV, respectively. In a similar way we may calculate the values of $\hbar^2/2\mathcal{J}$ and a for the $K=\frac{1}{2}^{+}$ band. Using experimental energies of levels of this band, we obtain 4.0 keV and -7.8, respectively.

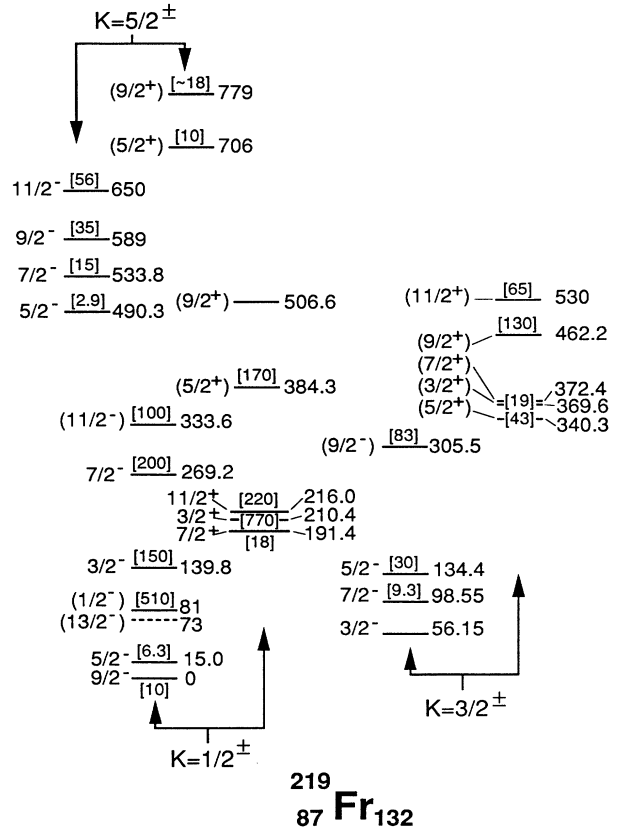

FIG. 6. Level structure for ^{219}Fr deduced from this experiment. Three sets of parity doublet bands are indicated, together with their K values and matrix elements. (See Fig. 8 and the text for a discussion of the matrix elements. Alpha-decay hindrance factors to the levels are given in square brackets.)

Not only are the decoupling parameters some of the largest known, but they are of opposite sign and similar in absolute value, as expected for a reflection asymmetric system. However, the decoupling parameters appear to be anomalously high. The decoupling parameter limits, as spherical shape is approached $[(-1)^{j-1/2}(j+\frac{1}{2})]$, suggest that the negative-parity $h_{9/2}$ orbital could approach a maximum decoupling parameter of $+5.0$. Since the positive-parity $i_{13/2}$ orbital has the decoupling parameter limit of $+7.0$ (i.e., the same sign as for the $h_{9/2}$ orbital), it cannot serve as the origin for the positive-parity partner to the $K=\frac{1}{2}^{-}$ intrinsic ground state of ^{219}Fr. Instead, we should search for this positive-parity partner in the low-spin positive-parity orbitals $s_{1/2}$ and $d_{3/2}$ from below the $Z=82$ gap [16]. The $s_{1/2}$ and $d_{3/2}$ orbitals have decoupling parameter limits of $+1.0$ and -2.0, respectively. These values do not appear to be good candidates for the explanation of the experimental value of -7.8 observed for the $K=\frac{1}{2}^{+}$ band in ^{219}Fr. Furthermore, the states originating from these orbitals are quite far from the Fermi surface.

In order to analyze this uncertainty in the decoupling parameters, it is necessary to know the structure of the low-lying states in ^{219}Fr in more detail. As was mentioned in the beginning of this paper, ^{219}Fr belongs to the group of nuclei where octupole modes of collective nuclear motion are energetically so low that stable nonzero octupole deformation (reflection-asymmetric deformation) is expected for the average nuclear field [16]. There are two alternative ways to treat these energetically very-low-lying collective octupole degrees of freedom and their coupling. First [16], the coupling between collective octupole modes and single-quasiparticle degrees of freedom is assumed to be very strong. This leads directly to an average nuclear field, which acquires stable reflection-asymmetric deformation. This is usually referred to in the literature as strong coupling. In the second alternative method, the average nuclear field is assumed to be in the standard reflection-symmetric form and the entire coupling between octupole and quasiparticle modes is treated as a residual interaction (intermediate coupling) [16]. The multiphonon excitation model [17] and quasiparticle phonon model [18] are microscopic variants of this intermediate-coupling scheme. In intermediate-coupling approaches there is no octupole deformation of the average field. However, as a consequence of very-low-energy octupole vibrations in neighboring even-even nuclei of ^{219}Fr, low-lying states in odd-A nuclei have large octupole phonon admixtures. We have chosen to use the intermediate-coupling model to investigate the microscopic structure of the levels in ^{219}Fr. We used the

standard axially symmetric rotor model [19] including Coriolis coupling. The intrinsic degrees of freedom are described by the quasiparticle phonon model [20]. In this approach the Hamiltonian can be written

$$H = H_{\text{inr}} + H_{\text{rot}} , \tag{1}$$

where H_{intr} represents the intrinsic part of the Hamiltonian and H_{rot} stands for the rotor Hamiltonian including the Coriolis term:

$$H_{\text{rot}} = (\hbar^2/2\mathcal{J})(\hat{I}^2 + \hat{j}^2 - \hat{I}_3^2 - \hat{j}_3^2) - (\hbar^2/2\mathcal{J})(\hat{I}_+\hat{j}_- + \hat{I}_-\hat{j}_+) . \tag{2}$$

In (2), $\mathcal{J}$ is the moment of inertia, $\hat{I}_3$ and $\hat{j}_3$ are projection operators of the total (**I**) and intrinsic (**j**) angular momenta, respectively, onto the nuclear symmetry axis, $\hat{I}_\pm = \hat{I}_1 \pm i\hat{I}_2$, and $\hat{j}_\pm = \hat{j}_1 \pm i\hat{j}_2$. In order to take into account the Coriolis coupling term [last term in (2)], the matrix of the total Hamiltonian (1) is constructed and diagonalized within the space of symmetrized functions:

$$|IMK\rho\rangle = [(2I+1)/16\pi^2]^{1/2} \times [D^I_{MK}|K,\rho\rangle + (-1)^{I+K} D^I_{M-K} R_i |K,\rho\rangle] . \tag{3}$$

Here D^I_{MK} are the Wigner functions of rotational angles and $|K,\rho\rangle$ represents the eigenvector of the intrinsic Hamiltonian, H_{intr} ($H_{\text{intr}}|K,\rho\rangle = E^{(\text{intr})}_\rho |K,\rho\rangle$). Here ρ are the quantum numbers of a given intrinsic state with projection K of the intrinsic angular momentum onto the symmetry axis. We approximate the intrinsic Hamiltonian with the quasiparticle model (QPM) Hamiltonian H_{QPM} [20], and so

$$H_{\text{intr}} \sim H_{\text{QPM}} , \quad |K,\rho\rangle \sim |\Psi_K(\rho)\rangle , \tag{4}$$

where $|\Psi_k(\rho)\rangle$ are eigenvectors of H_{QPM} [$H_{\text{QPM}}|\Psi_k(\rho)\rangle = \eta_\rho|\Psi_K(\rho)\rangle$]. H_{QPM} involves the average Nilsson reflection-symmetric field, pairing residual interaction and long-range residual interactions in quadrupole-quadrupole and octupole-octupole form [20]. The explicit formulas for H_{QPM} can be found in Refs. [18] and [20]. It should be noted that the long-range residual interactions in H_{QPM} contain (in addition to other parts) the coupling between octupole and quasiparticle degrees of freedom. The intrinsic wave function $|\Psi_K(\rho)\rangle$ in the QPM has one-quasiparticle components and one-quasiparticle–plus–phonon components [20]:

$$|\Psi_K(\tilde{\rho})\rangle = \left[\sum_\nu C^\rho_\nu \alpha^\dagger_\nu + \sum_{g\bar{\nu}} D^\rho_{\nu g} \delta_{\tilde{\mu}+\tilde{K}_\nu,\tilde{K}_\rho} \alpha^\dagger_{\bar{\nu}} Q^\dagger_g \right] \Bigg| \Bigg\rangle . \tag{5}$$

In (5), $\alpha^\dagger_{\bar{\nu}} = \alpha^\dagger_{\nu\sigma_\nu}$ represents the quasiparticle creation operator ($\sigma_\nu = \pm 1$ is the sign of the projection of the intrinsic angular momentum onto the intrinsic symmetry axis). The first term in (5) represents the sum over the one-quasiparticle components, each with amplitude C^ρ_ν. The second term in (5) involves the sum over quasiparticle-plus-phonon components. $Q^\dagger_g = Q^\dagger_{\lambda,\mu\sigma,i}$ stands for the creation operator of the phonons of the vibrating nuclear core with multipolarity λ and multipolarity projection $\tilde{\mu} = \mu\sigma$ ($\mu \geq 0$, $\sigma = \pm 1$). The index i enumerates the phonons with the same $\lambda\mu$. $D^\rho_{\nu g}$ represents the amplitude of the one-quasi-particle–plus–phonon component νg in the wave function (5). In each one-quasiparticle–plus–phonon component, the angular momentum projection of the odd particle is coupled with the angular momentum projection of the core phonon to the intrinsic angular momentum projection K ($\tilde{K}_\nu + \tilde{\mu} = \tilde{K}$). The symbol $|\,\rangle$ stands for the phonon as well as the quasiparticle vacuum. Expressions for the two-quasiparticle structure of the phonon creation operator $Q^\dagger_g$, for the amplitudes C^ρ_ν, $D^\rho_{\nu g}$, and for the corresponding intrinsic energy η_ν, is given in Ref. [20]. The decoupling parameter a_ρ for the state $|\Psi_{K=1/2}(\rho)\rangle$ is [20]

$$\begin{aligned} a_\rho &= -\langle \Psi_{K=1/2}(\rho)|j_+ R_i|\Psi_{K=1/2}(\rho)\rangle \\ &= \sum_\nu (C^\rho_\nu)^2 a_\nu(\text{Nilss}) \\ &\quad + \sum_\nu a_\nu(\text{Nilss})[(D^\rho_{\nu,20,i})^2 - (D^\rho_{\nu,30,i})^2] , \end{aligned} \tag{6}$$

where a_ν(Nilss) are the decoupling parameters calculated in the Nilsson single-particle scheme.

The analysis of the low-lying states in ^{219}Fr using the model described above involved the following steps.

(i) The eigenvalue problem $H_{\text{QPM}}|\Psi_K(\rho)\rangle = \eta_\rho|\Psi_K(\rho)\rangle$ was solved; the QPM intrinsic energies η_ρ and corresponding amplitudes C^ρ_ν, $D^\rho_{\nu g}$ were obtained. The Nilsson single-particle average field was used with its standard parametrization [21]. Deformation parameters were $\epsilon_2 = 0.08$ and $\epsilon_4 = -0.03$ [21,22]. All Nilsson shells with $N = 2-8$ were involved in the QPM calculation. The pairing gap parameter taken from Ref. [20] was $\Delta = 0.8$ MeV for protons and neutrons. Fermi energies for the proton and neutron systems were chosen in order to give the correct number of particles in each of these systems and were $\lambda_\rho = 43.549$ MeV and $\lambda_n = 49.917$ MeV. All parameters involved in the long-range residual interactions of H_{QPM} were determined by the energies of quadrupole and octupole core vibrations [10] of the neighboring even-even core [20]. In order to avoid the uncertainty connected with the choice of either the particle or hole even-even core, we used the averaged quadrupole and octupole vibrational energies of $^{218}_{86}$Rn and $^{220}_{88}$Ra. Specifically, we used $\hbar\omega_2 \sim 0.250$ MeV and $\hbar\omega_3 \sim 0.630$ MeV. The results of QPM calculations are presented in Table II. The first column of this table contains the percentages of the various components which make up the majority of the wave function (5) of specific intrinsic states. These include both the one-quasiparticle components ($|C^\rho_\nu|^2$) and the quasiparticle-plus-phonon components ($|D^\rho_{\nu g}|^2$). The second column of this table presents energies of the bandheads built on corresponding intrinsic [Eq. (5)]. The third column will be discussed later. The last column shows the calculated QPM intrinsic energies η_ρ (related to the intrinsic ground-state energy η_{ρ_0}).

(ii) In the second step the matrix elements of the opera-

TABLE II. Structure of the low-lying intrinsic states in ^{219}Fr.

Structure of the intrinsic state $\|\Psi_\rho(K)\rangle$		Experimental energy of the lowest level in rotational band (keV)	$E_\rho^{(\mathrm{intr})}-E_{\rho_0}^{(\mathrm{intr})}$ (keV)	$\eta_\rho-\eta_{\rho_0}$ (keV)
$\frac{1}{2}[541]$	87%			
$\frac{1}{2}[411]+Q_{30}^{+}$	2.2%			
$\frac{1}{2}[521]+Q_{20}^{+}$	2%			
$\frac{7}{2}[633]-Q_{33}^{+}$	1%			
$\frac{1}{2}[400]-Q_{31}^{+}$	1%	0.0 ($\frac{9}{2}^{-}$)	0.0	0.0
$\frac{1}{2}[411]$	32%			
$\frac{1}{2}[400]$	2.5%			
$\frac{1}{2}[541]+Q_{30}^{+}$	44%			
$\frac{3}{2}[532]-Q_{32}^{+}$	8%			
$\frac{1}{2}[541]-Q_{31}^{+}$	6%			
$\frac{5}{2}[523]-Q_{32}^{+}$	3%			
$\frac{3}{2}[532]-Q_{33}^{+}$	2%	191.3($\frac{7}{2}^{+}$)	242	292
$\frac{3}{2}[532]$	86%			
$\frac{3}{2}[402]+Q_{30}^{+}$	2%			
$\frac{7}{2}[514]-Q_{22}^{+}$	2%			
$\frac{3}{2}[512]+Q_{20}^{+}$	1.5%			
$\frac{1}{2}[411]+Q_{31}^{+}$	1.5%			
$\frac{9}{2}[614]-Q_{33}^{+}$	1%	56.15($\frac{3}{2}^{-}$)	35	10
$\frac{3}{2}[402]$	25%			
$\frac{3}{2}[651]$	2%			
$\frac{3}{2}[532]+Q_{30}^{+}$	30%			
$\frac{5}{2}[523]-Q_{31}^{+}$	22%			
$\frac{1}{2}[541]+Q_{31}^{+}$	8%			
$\frac{7}{2}[514]-Q_{32}^{+}$	7%	340.3 ($\frac{5}{2}^{+}$)	342	387
$\frac{5}{2}[523]$	75%			
$\frac{5}{2}[512]$	5%			
$\frac{1}{2}[541]+Q_{22}^{+}$	10%			
$\frac{1}{2}[411]+Q_{32}^{+}$	2%			
$\frac{3}{2}[402]+Q_{31}^{+}$	1.5%	325 ($\frac{5}{2}^{-}$)	288	215
$\frac{5}{2}[512]$	29%			
$\frac{5}{2}[523]$	2%			
$\frac{1}{2}[660]+Q_{32}^{+}$	13%			
$\frac{1}{2}[660]-Q_{33}^{+}$	11%			
$\frac{5}{2}[512]+Q_{20}^{+}$	11%			
$\frac{7}{2}[633]-Q_{31}^{+}$	7.5%			
$\frac{9}{2}[624]-Q_{32}^{+}$	4%	490.3 ($\frac{5}{2}^{-}$)	628	640
$\frac{5}{2}[402]$	25%			
$\frac{5}{2}[523]+Q_{30}^{+}$	17%			
$\frac{1}{2}[530]+Q_{32}^{+}$	13%			
$\frac{3}{2}[521]+Q_{31}^{+}$	11%			
$\frac{1}{2}[530]-Q_{33}^{+}$	8%			
$\frac{9}{2}[514]-Q_{32}^{+}$	7%	706 ($\frac{5}{2}^{+}$)	744	824

tors $\hat{j}_+$ and $\hat{j}^2$ between the intrinsic wave functions (5) are calculated. These matrix elements are needed for construction of the matrix of the total Hamiltonian H [see (1) and (2)].

(iii) The third step of the analysis of the low-lying states in ^{219}Fr consists in the construction and diagonalization of the matrix of the total Hamiltonian H using the basis function (3). In Coriolis mixing calculations it is usually sufficient to include in the basis of the functions $|IMK_\rho\rangle$ only those containing the lowest-energy intrinsic states $|\Psi_K(\rho)\rangle$. We took into account all functions $|IMK_\rho\rangle$ with intrinsic states originating from the $d_{3/2}$, $s_{1/2}$, and $i_{13/2}$ shells (for positive parity) and the $h_{9/2}$ and $f_{7/2}$ shells (for negative parity). The energies and wave functions of the levels of all rotational bands based on these intrinsic states were then obtained by diagonaliza-

tion of the total Hamiltonian matrix for each value of the total angular momentum and parity. Since the quasiparticle-plus-phonon model is *microscopic* without any free adjustable parameter for odd-A nuclei (all parameters are given by the even-even core), one cannot expect the intrinsic energies and decoupling parameters obtained from this model to correspond precisely to experiment. (The word "microscopic" is used here in the sense that the QPM provides also the two-quasiparticle structure of the core phonon in contrast to phenomenological models in which the question of phonon structure is *a priori* excluded.) Difficulties are also expected because the QPM is a "one-phonon" rather than a "multiphonon" model [17]. Therefore, in the Coriolis coupling calculations we treated the intrinsic energies $E_\rho^{(\mathrm{intr})}$ of the experimentally observed rotational bands as well as their decoupling parameters as free parameters. The QPM values for these quantities were used in the case of unobserved bands. The optimal values of the intrinsic energies $E_\rho^{(\mathrm{intr})}$ and the decoupling parameters (obtained from comparison of the experimental spectrum with the energies of the Coriolis mixing calculations) can be understood as the intrinsic experimental energies and decoupling parameters from which the rotational degrees of freedom have been removed. They can be directly compared with the corresponding QPM results, and so in our Coriolis mixing calculations the only free parameters were the intrinsic energies of observed bands, decoupling parameters of observed bands (when $K=\frac{1}{2}$), and the inertial parameters $\hbar^2/2\mathcal{I}$. We took the same value of the inertia parameter for all bands with the same parity. Thus we have five free parameters for each parity—a total of ten free parameters. We must therefore be cautious in assessing the degree of agreement between experiment and theory discussed below. It should, however, be noted that the main purpose in carrying out the Coriolis calculations was to obtain optimal values of the free parameters (free of Coriolis effects), which were then used in additional calculations of the structure of the intrinsic states in ^{219}Fr (Table II) discussed below.

The result of the Coriolis coupling calculations is shown in Fig. 7, where the calculated and experimental spectra are compared. The anomalous structures of the $K=\frac{1}{2}^{\pm}$ and $\frac{3}{2}^{\pm}$ PD bands are well reproduced by the calculations. The optimum values of the intrinsic energies $E_\rho^{(\mathrm{intr})}$ are given in the third column of Table II, where they are compared with QPM intrinsic energies η_ρ (the last column of Table II). The optimum values for inertial parameters were 4.2 keV for negative- and 4.7 keV for positive-parity bands. Comparison of the experimental values of the decoupling parameters of the $K=\frac{1}{2}^{\pm}$ bands observed in ^{219}Fr with decoupling parameters obtained by different theoretical methods is shown in Table III. The first row of this table contains the experimental values of the decoupling parameters (values obtained by fitting of the simple formula $E(I)=E_0+A[I(I+1)+a(-1)^{I+1/2}(I+\frac{1}{2})]$ to the experimental level energies for each band without Coriolis coupling). The spherical limit values $[(-1)^{j-1/2}(j+1/2)]$ are given in the second row (we assume that the main components of intrinsic states of $K=\frac{1}{2}^-$ and $\frac{1}{2}^+$ bands have their origin in $h_{9/2}$ and $d_{3/2}$ orbitals, respectively). Optimal values of decou-

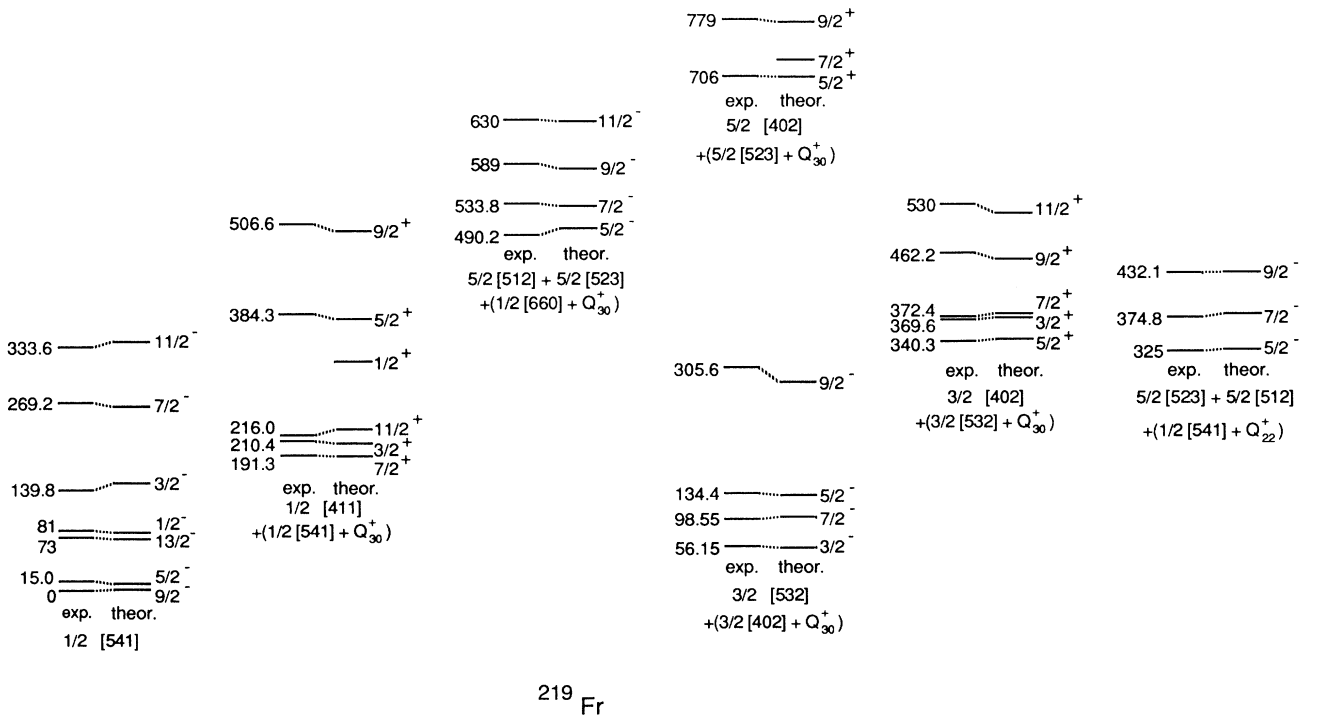

^{219}Fr

FIG. 7. Experimental and theoretical energies of the levels in ^{219}Fr. The experimental levels, shown to the left, are connected by a dotted line with the corresponding theoretical levels, shown to the right. Details of the Coriolis coupling calculations of the theoretical levels are given in the text.

TABLE III. Decoupling parameters of the lowest $K=\frac{1}{2}^{\pm}$ bands in ^{219}Fr obtained in experiment and by different theoretical schemes.

Calculation of decoupling parameter	Decoupling parameter of the lowest $K=\frac{1}{2}^{-}$ band	Decoupling parameter of the lowest $K=\frac{1}{2}^{+}$ band
Experimental value	7.03	−7.78
Spherical limit value	5.0 ($h_{9/2}$ orbital)	−2.0 ($d_{3/2}$ orbital)
Optimal value from Coriolis coupling calculation	6.0	−6.49
Nilsson value ($\epsilon_3=0.0$)	4.99 ($\frac{1}{2}$[541])	−1.99 ($\frac{1}{2}$[411])
Folded Yukawa value ($\epsilon_3=0.08$)	2.0 [$\frac{1}{2}(-0.1,-0.5,2)$]	−2.0 [$\frac{1}{2}(-0.1,-0.5,2)$]
Value from QPM	4.39	−2.82

pling parameters from Coriolis coupling calculations corresponding to Fig. 7 are presented in the third row. The fourth row contains the pure Nilsson decoupling parameters for the states $\frac{1}{2}$[541] and $\frac{1}{2}$[411], which form the main one-quasiparticle components in the corresponding intrinsic states (see Table II). The next row contains the decoupling parameters predicted by the reflection asymmetric single-particle folded Yukawa Hamiltonian. This Hamiltonian is connected with strong coupling of octupole and single-quasiparticle modes and will be discussed later. The decoupling parameters obtained from the quasiparticle-plus-phonon model by Eq. (6) are given in the last row.

One can see from Table II and Fig. 7 that, from the point of view of the intermediate-coupling scheme, using the QPM for description of the intrinsic degrees of freedom, the $K=\frac{1}{2}^{-}$ band has single-quasiparticle character with the major component ($\frac{1}{2}$[541]) originating from the $h_{9/2}$ orbital, while the $K=\frac{1}{2}^{+}$ band is mainly created by the octupole core vibration coupled to the odd proton in the $\frac{1}{2}$[541] quasiparticle state. The intrinsic $K=\frac{1}{2}^{+}$ state also has a fairly large $\frac{1}{2}$[411] single-quasiparticle component originating from the $d_{3/2}$ orbital. This structure of intrinsic $K=\frac{1}{2}^{\pm}$ states gives the value of decoupling parameters given in the sixth row of Table III. These values are low in comparison with the values given in the third row of Table III necessary for reproducing the experimental spectrum. However, it must be remembered that the structure of the intrinsic states in the QPM is quite sensitive to the single-quasiparticle spectrum used in the calculation. Since there is evidence [21] that the real experimental picture of the single-quasiparticle spectrum in the vicinity of the Fermi surface is sometimes quite different from that given by the Nilsson or Saxon-Woods schemes, one would assume that the real single-quasiparticle proton spectrum is organized so that the positive-parity member of the $K=\frac{1}{2}^{\pm}$ doublet is almost entirely formed by the ($\frac{1}{2}$[541]$+Q_{30}^{+}$) component. In such a case, formula (6) gives ~ -4.9 for the decoupling parameter of the $K=\frac{1}{2}^{+}$ band (the same absolute value with opposite sign as that for the $K=\frac{1}{2}^{-}$ band), and this value is closer to values in the third column of Table III. This possibility of interpretation of the $K=\frac{1}{2}^{\pm}$ doublet is also mentioned in Ref. [17] in the description of the ^{221,223}Ac isotopes.

In the case of $K=\frac{3}{2}^{\pm}$ and $\frac{5}{2}^{\pm}$ doublets, the QPM also predicts strong octupole collective components for the positive-parity member of the doublet, while the negative-parity partners are less collective and have their origin in $h_{9/2}$ or $f_{7/2}$ orbitals.

It is, however, quite significant that in several cases involving positive-parity band members of the parity doublets, significant contributions of the microscopic structure result from Nilsson states occurring in the shell below.

An alternative description of the intrinsic states in ^{219}Fr is based on the strong-coupling scheme [23] in which the octupole core is coupled to the quasiparticle states of the odd proton calculated from a single-particle folded Yukawa potential with reflection asymmetry $\epsilon_3=0.08$. A plot [23] of these levels versus quadrupole deformations is shown in Fig. 8. They are labeled by Ω and in parentheses by the single-particle matrix elements $\langle\hat{s}_z\rangle$, $\langle\hat{\pi}\rangle$, and for $K=\frac{1}{2}$ bands only

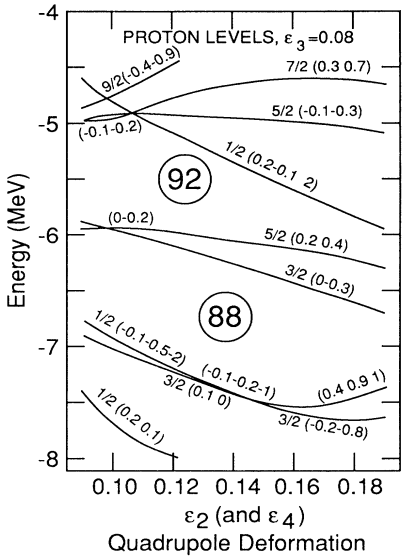

FIG. 8. Single-proton orbitals in an axially symmetric but reflection asymmetric folded Yukawa potential with $\epsilon_3=0.08$ plotted against the quadrupole deformation ϵ_2 (and ϵ_4). The orbitals are labeled by Ω and, in parentheses, a set of single-particle matrix elements (see text). Proton numbers are indicated in circles. The function $\epsilon_4(\epsilon_2,\epsilon_3)$ is given in Table I of Ref. [16].

$\langle \pi \text{ conj}| -\hat{j}_+ |R \text{ conj}\rangle$. The ground state of ^{219}Fr with 87 protons (assuming a quadrupole deformation $\epsilon_2=0.08$) is predicted by Fig. 8 to give the observed parity doublet $K=\frac{1}{2}^{\pm}$ from the configuration $\frac{1}{2}(-0.1,-0.5,2)$. Almost degenerate with the $K=\frac{1}{2}^{\pm}$ PD bands, Fig. 8 suggests a second set of observed PD bands with $K=\frac{3}{2}^{\pm}$ and configuration $\frac{3}{2}(0.1,0)$. The third set of observed PD bands with $K=\frac{5}{2}^{\pm}$ and configuration $\frac{5}{2}(0,-0.2)$ is also predicted by Fig. 8. Thus, not only their presence, but also the energy ordering of the three sets of PD bands is explained by Fig. 8.

The four unassigned levels in Fig. 5 include two tentative levels at 325 and 445 keV, which are populated in the alpha decay of ^{223}Ac, but are not experimentally observed to depopulate. In addition, there are two levels at 374.8 and 432.1 keV with depopulating gammas which allow some possible spin assignments. Very tentatively (on the

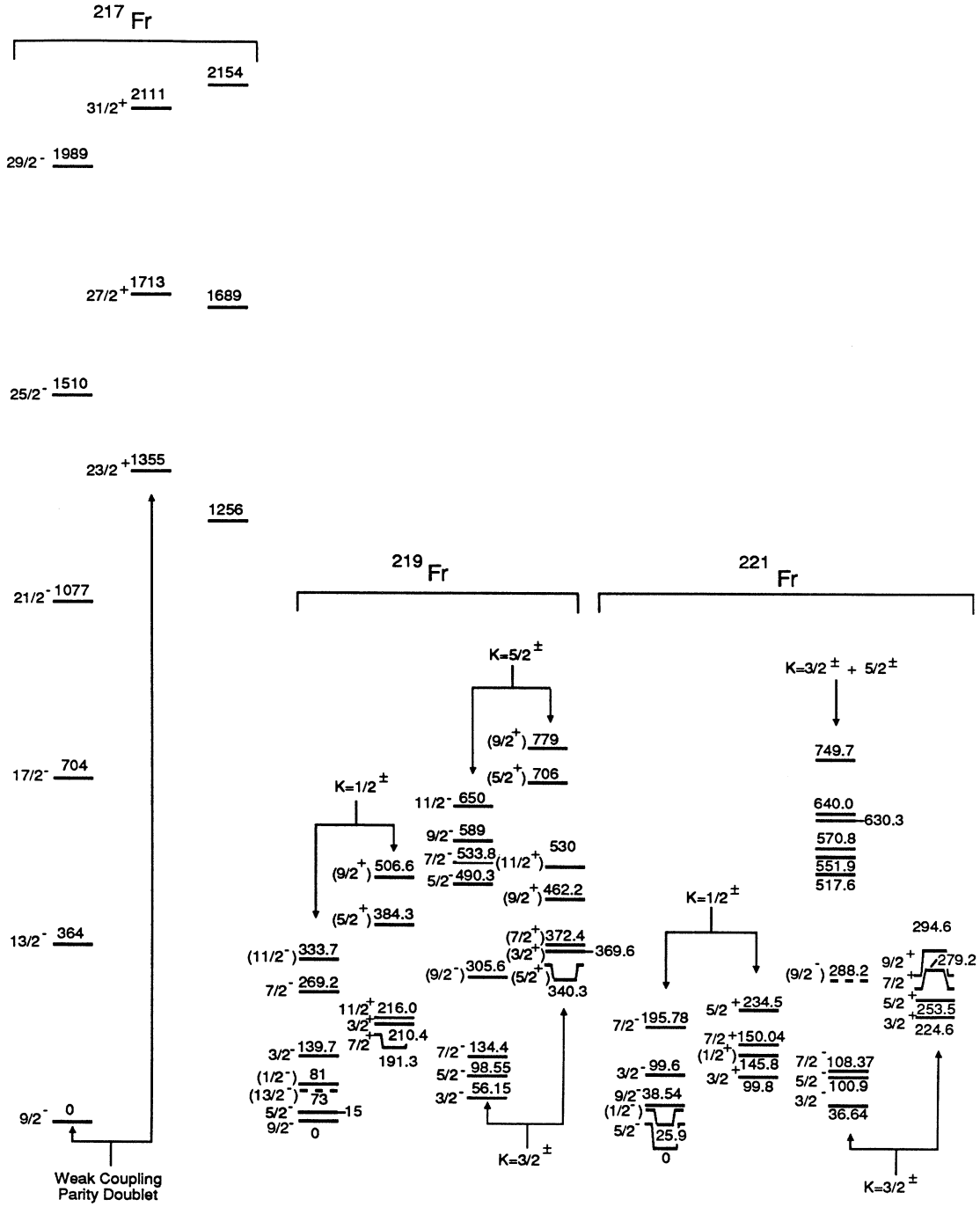

FIG. 9. Comparison of the level structures of ^{217}Fr (left), ^{219}Fr (center), and ^{221}Fr (right). Spins and parities are shown to the left of each level and energies above or below the level. Double sets of arrows show parity doublet bands.

basis of the simple comparison of the QPM results with the experimental spectrum), we suggest that these levels may be part of the rotational band built on the mixture of $\frac{5}{2}[523], \frac{5}{2}[512]$ single-quasiparticle states and the gamma vibration built on the $\frac{1}{2}[541]$ state as is implied in Fig. 7 and Table II. In the language of strong coupling, it is probably a gamma vibrational band built on the $\frac{1}{2}(-0.1, -0.5, 2)$ reflection-asymmetric proton orbital.

In spite of the anomalous character of the $K=\frac{1}{2}^{\pm}$ and $\frac{3}{2}^{\pm}$ level spacings, it is of interest to note that the level spacing in the $K=\frac{5}{2}^{-}$ member of the $K=\frac{5}{2}^{\pm}$ parity doublet set is reasonably regular. The hindrance factors for the $\frac{5}{2}^{-}$ to $\frac{11}{2}^{-}$ states go through the regular sequence 2.9, 15, 35, and 56, while the values of $\hbar^2/2\mathcal{J}$ for the $\frac{7}{2}^{-}$ to $\frac{5}{2}^{-}$, $\frac{9}{2}^{-}$ to $\frac{7}{2}^{-}$, and $\frac{11}{2}^{-}$ to $\frac{9}{2}^{-}$ spacings are 6.51, 5.96, and 5.49 keV, respectively. The entire band fits well energetically with an $I(I+1)$ formalism when one includes a moderately large rotation-vibration interaction term.

Figure 9 compares the lower-lying spectrum of ^{217}Fr [7] with ^{219}Fr (from this research) and ^{221}Fr [8]. The difference between ^{217}Fr, on the one hand, and ^{219}Fr and ^{221}Fr on the other is immediately obvious. Whereas ^{217}Fr has a typical weak-coupling spectrum with the $\frac{9}{2}^{-}$ proton coupled core of the even-even nucleus ^{218}Ra, both ^{219}Fr and ^{221}Fr have strong-coupling spectra which can be explained in terms of a quadrupole-octupole deformed system modeled in Fig. 8.

In spite of these spectral differences, the states of alternating parity in ^{217}Fr are connected by $E1$ transitions which are considerably enhanced [$B(E1)=2\times10^{-3}$ W.u.] compared with those in other regions of the periodic table. This supports the assumption of a static octupole deformation similar to that in ^{219}Fr and ^{221}Fr. It may well be that the major difference in the sequence ^{217}Fr,^{219}Fr,^{221}Fr is a gradually increasing quadrupole deformation. One is therefore forced to ask the question whether it is the mode of population which is the determining factor in the spectral differences observed or the underlying nuclear shapes.

The spectrum of ^{217}Fr shown in Fig. 9 is that resulting from the reaction ^{210}Pb(^{11}B,4n). This heavy-ion reaction is expected to populate high-spin Yrast states. On the other hand, the spectra of ^{219}Fr and ^{221}Fr result from the alpha decay of the $\frac{3}{2}^{-}$ and $\frac{5}{2}^{-}$ ground states of ^{223}Ac and ^{225}Ac, respectively. These relatively low-spin Ac ground states can only populate moderately low-spin states in ^{219}Fr and ^{221}Fr.

Is it possible that both weak- and strong-coupling spectra exist in the same transitional nuclei and the mode of population determines what we observe? To check this out we need to utilize both modes of population in the same nucleus. Unfortunately, the spectroscopic data from the alpha decay of ^{221}Ac into ^{217}Fr are so meager that there is no meaningful overlap with the spectral data from the heavy-ion reaction. Since there are no heavy-ion reaction data populating states in ^{219}Fr and ^{221}Fr, this must remain an open question. However, these detailed spectroscopic data on ^{218}Fr following alpha decay provide a basis for comparison with future heavy-ion spectroscopy in ^{219}Fr.

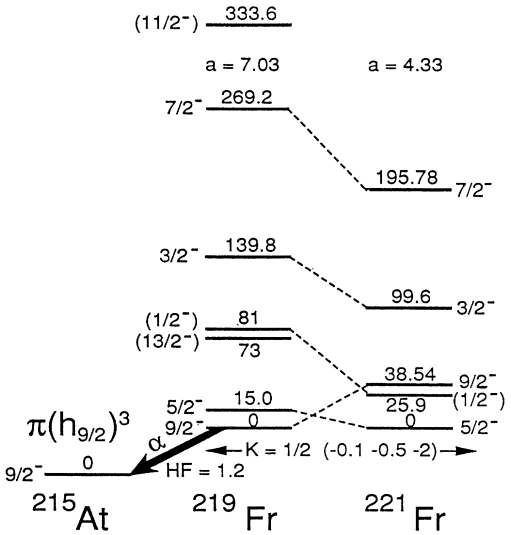

FIG. 10. Comparison of the experimental $K=\frac{1}{2}^{-}$ bands in ^{219}Fr and ^{221}Fr, showing the effect of the larger decoupling parameter in producing the $\frac{9}{2}^{-}$ ground state in ^{219}Fr. The alpha decay of the resulting $\frac{9}{2}^{-}$ ground state of ^{219}Fr into the $\frac{9}{2}^{-}$ ground state of ^{215}At with a very low hindrance factor is also indicated.

Finally, it is of considerable interest to attempt to understand the mechanism by which the collapse of Nilsson-like states into shell-model-like states occurs as we go from the well-deformed actinides toward the double closed shell in ^{208}Pb. One very interesting aspect of this effect is shown in Fig. 10. This figure compares the lowest-lying levels in ^{219}Fr with those in ^{221}Fr [8]. Figure 10 demonstrates clearly that the $K=\frac{1}{2}^{-}$ band member of the $\frac{1}{2}(-0.1, -0.5, -2)$ configuration is changing drastically as the quadrupole deformation decreases in going from ^{221}Fr to ^{219}Fr. The larger decoupling parameter in ^{219}Fr (7.03) compared to that in ^{221}Fr (4.33) [8] causes the $\frac{9}{2}^{-}$ state to become the ground state as the quadrupole deformation decreases. This is, of course, expected since decreasing quadrupole deformation will increase the decoupling parameter and the Coriolis coupling with the $K=\frac{3}{2}^{-}$ band. In any case, it is the increasing value of the decoupling parameter of the $K=\frac{1}{2}^{-}$ band which drives the $\frac{9}{2}^{-}$ state down to become the ground state. Furthermore, the hindrance factor (1.2) [10] for the alpha decay of the ^{219}Fr ground state to the ($h_{9/2}$) [3] ^{215}At ground state (see Fig. 10) implies that this $\frac{9}{2}^{-}$ ^{219}Fr ground state, while still a legitimate member of the $K=\frac{1}{2}^{-}$ band, also has considerable $h_{9/2}$ character expected for a spherical ground state.

ACKNOWLEDGMENTS

We are indebted to J. Obert and J. C. Putaux for collaboration in the mass separations. One of us (R.K.S.) wishes to thank the National Science Foundation for support under Contract No. PHY89-06613 with Florida State University.

[1] P. D. Cottle, M. Gai, J. F. Ennis, J. F. Shriner, D. A. Bromley, C. W. Beausang, L. Hildingsson, W. F. Piel, D. B. Fossan, J. W. Olness, and E. K. Warburton, Phys. Rev. C **33**, 1855 (1986); **36**, 2286 (1987).

[2] S. Khazrouni, A. Chevallier, J. Chevallier, O. Helene, G. Ramanantsizehena, and N. Schulz, Z. Phys. **320**, 535 (1985).

[3] M. W. Drigert and J. A. Cizewski, Phys. Rev. C **31**, 1977 (1985).

[4] J. Fernandez-Niello, H. Puchta, F. Riess, and W. Trautmann, Nucl. Phys. **A391**, 221 (1982).

[5] M. Gai, J. F. Ennis, M. Ruseev, E. C. Schloemer, B. Shivakumar, S. M. Sterbenz, N. Tsoupas, and D. A. Bromley, Phys. Rev. Lett. **51**, 646 (1983).

[6] Y. Gono, T. Kohno, M. Sugawara, Y. Ishikawa, and M. Fukuda, Nucl. Phys. **A459**, 427 (1986).

[7] M. Aiche, A. Chevallier, J. Chevallier, S. Hulne, S. Khazrouni, N. Schulz, and J. C. Sens, J. Phys. G **14**, 1191 (1988).

[8] R. K. Sheline, Phys. Lett. B **205**, 11 (1988); C. F. Liang, A. Peghaire, and R. K. Sheline, Mod. Phys. Lett. A **5**, 1243 (1990).

[9] C. F. Liang, P. Paris, Ch. Briançon, and R. K. Sheline, Int. J. Mod. Phys. A **5**, 1551 (1990).

[10] C. M. Lederer and V. S. Shirley, *Table of Isotopes*, 7th ed. (Wiley, New York, 1978); C. Maples, Nucl. Data Sheets **22**, 223 (1977).

[11] C. F. Liang (unpublished).

[12] C. F. Liang, P. Paris, and R. K. Sheline, Nucl. Phys. **A520**, 361c (1990).

[13] C. F. Liang, P. Paris, D. Bucurescu, S. Bellahegra, J. Obert, and J. C. Putaux, Z. Phys. A **309**, 185 (1982).

[14] C. F. Leang, thesis, Université de Paris-Sud, 1969.

[15] R. K. Sheline, C. F. Liang, and P. Paris, Int. J. Mod. Phys. A **5**, 2821 (1990); R. K. Sheline, P. C. Sood, C. F. Liang, P. Paris, and R. W. Hoff, *ibid.* **5**, 2833 (1990).

[16] G. A. Leander and Y. S. Chen, Phys. Rev. C **37**, 2744 (1988).

[17] R. Piepenbring, Z. Phys. A **323**, 341 (1986); V. Leandri and R. Piepenbring, Phys. Rev. C **37**, 2779 (1988).

[18] V. G. Soloviev, Z. Phys. A **324**, 393 (1986); V. G. Soloviev, V. O. Nesterenko, and S. I. Bastrukov, *ibid.* **309**, 353 (1983); V. O. Nesterenko, *ibid.* **335**, 147 (1990).

[19] J. Kvasil, T. I. Kraciková, M. Finger, and B. Choriev, Czech. J. Phys. B **31**, 1376 (1981); **33**, 626 (1983); **35**, 1084 (1985); **36**, 581 (1986).

[20] V. G. Soloviev, *Theory of Complex Nuclei* (Pergamon, Oxford, 1976).

[21] A. K. Jain, R. K. Sheline, P. C. Sood, and K. Jain, Rev. Mod. Phys. **62**, 393 (1990).

[22] S. G. Nilsson, C. F. Tsang, A. Sobiczewksi, S. Wycech, C. Gustafson, I. L. Lamm, P. Möller, and B. Nilsson, Nucl. Phys. **A131**, 1 (1969).

[23] G. A. Leander and R. K. Sheline, Nucl. Phys. **A413**, 375 (1984).